

PIGEON: Predicting Image Geolocations

Lukas Haas¹ Michal Skreta¹ Silas Alberti²

Extended Abstract

Planet-scale image geolocation remains a challenging problem, necessitating fine-grained understanding of visual information across countries, environments, and time. Although traditional retrieval-based approaches using hand-crafted features have recently been superseded by deep learning methods, transformer-based advances in machine learning have rarely been applied in image geolocation.

We introduce PIGEON, a novel deep multi-task model for planet-scale Street View image geolocation that incorporates, *inter alia*, semantic geocell creation with label smoothing, conducts pretraining of a CLIP vision transformer on Street View images, and refines location predictions with ProtoNets across a candidate set of geocells. Our work presents three major contributions: first, we design a semantic geocells creation and splitting algorithm based on open-source data which can be adapted to any geospatial dataset. Second, we show the effectiveness of intra-geocell few-shot refinement and the applicability of unsupervised clustering and ProtNets to the task. Finally, we make our pre-trained CLIP transformer model, StreetCLIP, publicly available for use in adjacent domains with applications to fighting climate change and urban and rural scene understanding.

Motivated by the rising popularity of an online game GeoGuessr with over 50 million players worldwide, we focus specifically on Street View images and create the first AI model which consistently beats human players in GeoGuessr, ranking in the top 0.01% of players.

In addition to our novel modeling approach, we create a new planet-scale dataset for image geolocation of 400,000 images. Our model achieves impressive results, aided by positive multi-task transfer in both an implicit and explicit multi-task setting. We attain 91.96% country accuracy on our held-out set and 40.36% of our guesses are within 25 km of target.

One of the most important results of our work is demonstrating the domain generalization of our pre-trained CLIP model called StreetCLIP (Haas et al., 2023) and its robustness to distribution shifts. We apply StreetCLIP in a zero-shot fashion to out-of-distribution benchmark datasets IM2GPS and IM2GPS3k and achieve state-of-the-art results, beating models finetuned on more than four million in-distribution images.

Finally, we show that contrastive pretraining is an effective meta-learning technique for image geolocation with StreetCLIP realizing a more than 10 percentage points accuracy increase over CLIP on countries not seen during StreetCLIP-specific pretraining. With image geolocation datasets varying widely in terms of geographical distribution, our results demonstrate the effectiveness of applying StreetCLIP to any geolocation and related problem.

1. Introduction

The game of GeoGuessr has become a worldwide sensation in the recent years, attracting over 50 million players globally and getting covered by the New York Times (Browning,

2022). On its surface, GeoGuessr seems quite simple: given a Street View location, players need to say where they find themselves in the world. Yet despite this seeming simplicity, the game is infamously difficult. As a result of the diversity of countries, seasons, and climates in the world, it is very hard for most humans to accurately pinpoint their locations.

Motivated by Geoguessr, we embarked on finding a state-of-the-art approach to planet-scale image geolocation. The general problem of photo geolocation has a variety of popular use cases, ranging from geographic photo tagging and retrieval at large technology companies to academic, historical research based on archival images. The societal

¹Department of Computer Science, Stanford University, Stanford, CA, USA. ²Department of Electrical Engineering, Stanford University, Stanford, CA, USA. Correspondence to: Lukas Haas <lukashaas@cs.stanford.edu>, Michal Skreta <michal.skreta@stanford.edu>, Silas Alberti <salberti@stanford.edu>.

interest in artificial intelligence being able to recognize location from images became clear in 2016, when a paper published by Google garnered worldwide coverage by the media (Weyand et al., 2016). Given the rising popularity of GeoGuessr, numerous amateur attempts have been made at “solving” the game (Suresh et al., 2018; de Fontnouvelle, 2021; Cassens, 2022). There is also an additional incentive to contribute to a growing community of geography enthusiasts, with AI models having the potential to improve geography education and the potential of the learned Street View representations to be beneficial for applications in sustainability, i.e. the prediction of buildings’ energy efficiency (Mayer et al., 2022).

In this work, we present PIGEON, a model trained on Street View data drawn from the same distribution as GeoGuessr, achieving an impressive image geolocation results and consistently beating humans in the game of GeoGuessr, ranking amongst the top players globally. Some of our work’s major contributions revolve around the use of CLIP, a recent multi-modal vision transformer which has been shown to be an effective few-shot learner (Radford et al., 2021), which is important given the geographical sparsity of images in most image geolocation datasets. As such, our work innovates on approaches still leveraging convolutional neural networks (CNNs) such as (Weyand et al., 2016).

The remainder of this paper proceeds as follows. In Section 2, we outline past approaches to the problem of image geolocation. In Section 3, we describe our dataset and the process of acquiring and augmenting our data. In Section 4, we discuss our proposed approach, outlining the six-step process comprising PIGEON. In Section 5, we present our results, discussing both distance-based metrics pertaining to our main image geolocation task as well as other metrics relevant for our augmented dataset. In Section 6, we analyze the particularities of the performance of our model while attempting to interpret some predictions of the model. Section 7 summarizes our work, and Section 8 outlines potential future directions for our research.

2. Related Work

2.1. Traditional Image Geolocation

The task of image geolocation, also referred to as visual place recognition (Berton et al., 2022a), is typically described as a difficult problem due to the sheer diversity of the conditions in which images are taken. An image can be taken during daytime or nighttime, with varying weather, illumination, season, traffic, occlusion, viewing angle, and many other factors. In fact, the task is deemed so difficult that it was not immediately clear that visual features could have superior predictive power in localizing images than textual features (Crandall et al., 2009).

What is perhaps even more challenging, however, is the fact that images can be taken anywhere in the world, representing an extremely vast classification space. To that end, many of the previous approaches at image geolocation were constrained to small types of parts of the world, such as looking exclusively at cities (Wu & Huang, 2022), specific mountain range like the Alps (Baatz et al., 2012; Saurer et al., 2016; Tomešek et al., 2022), deserts (Tzeng et al., 2013), or even beaches (Cao et al., 2012). Other approaches focused on highly constrained geographical area, such as the United States (Suresh et al., 2018) or even specific cities like Pittsburgh and Orlando (Zamir & Shah, 2010) or San Francisco (Berton et al., 2022a).

The first modern attempt at planet-scale image geolocation is attributed to IM2GPS in 2008 (Hays & Efros, 2008), a retrieval-based approach using nearest-neighbor search based on hand-crafted features. It was the first time that image geolocation was considered in an unconstrained manner on a global scale. Yet despite this scale, dependence on nearest-neighbor retrieval methods (Zamir & Shah, 2014) meant that an enormous database of reference images would be necessary for accurate image geolocation on the scale of the entire planet.

2.2. Deep Image Geolocation

2.2.1. CONVOLUTIONAL NEURAL NETWORKS (CNNs)

Interest in image geolocation surged with the arrival of deep learning to computer vision, marking an evolution from hand-crafted to deep-learned features (Masone & Caputo, 2021). In 2016, Google released a paper called PlaNet (Weyand et al., 2016) that first applied convolutional neural networks (CNNs) (Krizhevsky et al., 2012) to photo geolocation. It also first cast the problem as a classification task, which was particularly important as past research has shown that it was difficult for deep learning models to directly predict geographic coordinates (de Brebisson et al., 2015) because most models do not learn the distributions of data points efficiently, as well as because of the interdependence of latitude and longitude. The improvements made with deep learning led researchers to revisit IM2GPS (Vo et al., 2017), apply CNNs to massive datasets on mobile images (Howard et al., 2017), and make applications to GeoGuessrs more widespread (Suresh et al., 2018; Luo et al., 2022). Nevertheless, some researchers argue for using approaches combining classification and retrieval (Kordopatis-Zilos et al., 2021).

2.2.2. VISION TRANSFORMERS

Following the success of transformers (Vaswani et al., 2017) in natural language processing, the transformer architecture found its application to computer vision, such as through the ViT architecture (Kolesnikov et al., 2021). The global

context of ViT architectures explains immediate significant improvements compared with CNNs (Raghu et al., 2021). Additionally, vision transformers have been found to be useful in multi-model text and image setting, such as through the OpenAI’s CLIP model (Radford et al., 2021) being applied to image geolocalization (Wu & Huang, 2022; Luo et al., 2022). Prior papers have also used contrastive learning without the use of CLIP (Kordopatis-Zilos et al., 2021).

Although vision transformers have been successfully applied to a range of problems in Computer Science, applications of these models have thus far been fairly limited (Pramanick et al., 2022), but have recently been accelerating (Bertón et al., 2022b). In particular, the emergence of vision transformer models has not been widely applied to the problem of geolocalization from Street View imagery.

2.3. Multi-task Image Geolocalization

Multi-task approaches have been found to be improving results of the main task by using complementary tasks (Ranjan et al., 2016), with certain types of task being more beneficial for the main task than others (Bingel & Søgaard, 2017). This, coupled with the fact that auxiliary information was found to be a vital pre-processing step for image geolocalization (Pramanick et al., 2022), pointed to the potential of multi-task learning to significantly accelerated the field of image geolocalization.

Extracting sets of priors about objects that can potentially be seen in an image (Ardeshir et al., 2014) can be framed as ingredients to a multi-task setting, such as by using scene recognition as a secondary task in a multi-task framework (Pramanick et al., 2022). By using semantic segmentation, the problem of extreme variation can be alleviated (Seymour et al., 2018). In fact, until recently, state-of-the-art performance (Müller-Budack et al., 2018) was made possible by combining convolutional neural networks with contextual information about environmental scenes. This is particularly important as image geolocalization is very difficult in natural environments (Tomešek et al., 2022). More recent work showed that vision transformers and multi-task settings (Pramanick et al., 2022) contribute to superior performance, further accelerating research in the field.

2.4. Geocell Partitioning

The chosen method of partitioning the world into geocells can have an enormous effect on downstream classification performance. Previous approaches rely on geocells that are either plainly rectangular (de Fontnouvelle, 2021), rectangular using the S2 library (Müller-Budack et al., 2018), or effectively arbitrary, such as through combinatorial partitioning (Seo et al., 2018). While semantic construction of geocells has been found to be of high importance to image geolocalization (Theiner et al., 2022), even current state-of-

the-art papers using the S2 library (Pramanick et al., 2022). Alternative method for achieving optimized geocells include creating specific loss functions for the classification layer (Izbicki et al., 2019).

2.5. Additional Prior Work

Other prior academic work cited the need for cross-view image geolocalization as photos tend to be concentrated in landmarks and urban areas with sparse ground level geo-tagged photos. Cross-view approaches can combine ground-level appearance, overhead appearance, and land cover attributes (Lin et al., 2013). What is more, methods using Street View images have shown incredible potential in inferring factors such as income, race, education, and voting patterns (Gebru et al., 2017). In prior work, oftentimes the Street View images were inputted to the model in conjunction with images of landmarks (Weyand et al., 2020), images taken indoors, or cross-viewed with aerial images (Yang et al., 2021; Zhu et al., 2022). Moreover, recent paper cited the potential of also geolocalizing objects within images (Wilson et al., 2021), factoring in the differences in land cover (Rußwurm et al., 2020), and setting new benchmarks (Bertón et al., 2022b). Further information about work done in image geolocalization can be found in various surveys of the field (Masone & Caputo, 2021; Wilson et al., 2021; Mai et al., 2022; Li & Hsu, 2022).

3. Dataset

3.1. Dataset Acquisition

While most image geolocalization approaches rely on publicly available datasets, this is not the case for Street View given the lack of publicly available planet-scale Street View datasets.

To that end, we decided to create on original dataset. We proactively reached out to Erlend Ranvinge, the Chief Technology Officer of Geoguessr, who generously agreed to share a dataset of 1 million locations used in the Competitive Duels mode of GeoGuessr. From the dataset, we randomly sampled 100,000 of the provided locations, or 10% of the overall dataset. For each of the locations, we downloaded four images, ending up with 400,000 images.

The distribution of countries in our training set is displayed in Figure 20 in Section B of the Appendix. It is also where the details about our process of querying the Street View API, including relevant parameters for both Street View metadata and Street View images, is described. As can be seen, there are clear “tiers” of countries delineated by the frequency of sampling, and we denote each tier by a different color. Approximately 70% of the locations are in the “high” tier, 24% are in the “medium” tier, and the remaining 6% are in the “low” tier.

For each location, we start with a random compass direction and take four images separated by 90 degrees, thus differing from a single-image setup typically seen in Street View image geolocalization (de Fontnouvelle, 2021). We carefully created non-overlapping image patches like in prior approaches (Cassens, 2022), and cropped images to remove auxiliary watermarks.

Prior work addressing using Street View for GeoGuessr image geolocalization did not specifically look at data obtained directly from the GeoGuessr game (Luo et al., 2022), making our approach particularly novel.

3.2. Image Format

Four images for a sample location in our dataset are visualized in Figure 1. It is crucial to notice the advantage of a four-image setting compared to a single-image setting. Looking at the leftmost image in Figure 1, it mainly contains information on vegetation, making it difficult to locate the image with confidence. However, the additional images provide clues pertaining to roads, buildings and cars, pointing to the advantages of extending the dataset with additional images in lieu of taking a single image for each location.

3.3. Dataset Augmentation

Recognizing that adding auxiliary geographic metadata can be beneficial for image geolocalization (Arbinger et al., 2022), we decided to augment our dataset with data on Köppen-Geiger climate zones (Beck et al., 2018), as well as elevation, temperature, precipitation, etc. We also capture information frequently used by human GeoGuessr players in placing their guesses such as the side of the road that traffic travels on.

Details regarding specific datasets used in our dataset augmentation procedure are described in Section A of the Appendix.

4. Methodology

This work introduces a variety of technical novelties applied to the problem of image geolocalization, summarized in the following subsections.

4.1. Geocell Creation

Prior research has shown that predicting latitudes and longitudes directly for any image geolocalization problem does not result in state-of-the-art performance (Theiner et al., 2022). Current methods all rely on the generation of geocells to discretize the coordinate regression problem and thus transform it into a classification setting, making geocell design “crucial for performance” (Theiner et al., 2022).

4.1.1. NAIVE GEOCELLS

Our initial geocell design is inspired by the approach undertaken by papers that had previously achieved state-of-the-art result on image geolocalization (Müller-Budack et al., 2018; Pramanick et al., 2022) using the S2 geometry library. The S2 geocell algorithm uses numerous rectangles which observe the curvature of the earth and split each rectangle into four equally-sized smaller rectangles if the number of data points within a given rectangle reaches a pre-defined threshold. Our naive geocell algorithm works in a similar fashion; it is first initialized with one large rectangle which is in every subsequent step divided into two rectangles along the longest side, only dividing a rectangle further if the two resulting rectangles contain a minimum of thirty points. Instead of splitting each rectangle into two equally-sized rectangles, a k -means clustering is performed with $k = 2$ to find a decision boundary, only splitting the given rectangle if the minimum geocell size of thirty training data points is respected. Figure 2 illustrates the resulting rectangular geocells derived from our naive geocell creation algorithm for the metropolitan area of Paris.

4.1.2. SEMANTIC GEOCELLS

A major contribution of this work is our contribution on the generation of semantic geocells which automatically adapt based on the geographic distribution of any training dataset samples. The motivation behind a semantic geocell design is that visual features in images often follow the semantics of the given country (i.e. road marking), region (i.e. quality of infrastructure), or city (i.e. street signs). In addition, country or administrative boundaries often follow natural borders such as the flow of rivers or mountain ranges which in turn influence visual features such as the type of vegetation, soil color, or more.

We use planet-scale open-source administrative data for our semantic geocell design, relying on non-overlapping political shape files of three levels of administrative boundaries (country, admin 1, and admin 2 levels) obtained from (GADM, 2022). Starting at the most granular level (admin 2), our algorithm merges adjacent admin 2 level polygons to such that each geocell contains at least thirty training samples. Our method attempts to preserve the hierarchy given by admin 1 level boundaries and never merges cells across country borders (defined by distinct ISO country codes). It randomly merges geocells with adjacent cells using the following prioritization:

1. Small adjacent geocells in same admin 1 area.
2. Large adjacent geocells in same admin 1 area.
3. Small adjacent geocells in same country.
4. Large adjacent geocells in same country.



Figure 1. Four images comprising a 360-degree panorama in Pegswood, England in our dataset.

The above prioritization of our algorithm ensures that geocells containing fewer than the minimum threshold of training samples are not simply appended to large adjacent geocells but instead results in low-density regions being aggregated into one larger cell, often surrounding major metropolitan areas. This further preserves rural and urban semantics. Figure 2 shows an example of our semantic geocell design preserving the urban area of Paris as well as the surrounding sub-urban regions.

One limitation of aggregating admin 2 level areas as defined by (GADM, 2022) is that for some urban areas, the number of training examples for a single cell might greatly exceed the minimum sample threshold defined by the algorithm’s user. In addition, through the process of merging adjacent geocells, some cells might be created which could be split again into multiple smaller cells based on different boundaries.

We address this limitation in our geocell design through the following innovative algorithm which uses Voronoi Tessellation and the OPTICS clustering algorithm (Ankerst et al., 1999) to further split a geocell into further smaller semantic geocells.

Our Semantic Geocell Division Algorithm uses OPTICS (Ankerst et al., 1999) to find a large cluster within a cell, checking whether removing this cluster from the cell would result in two cells each having a large number of training samples than MINSIZE. If this is the case, the new geocell’s polygon is determined by performing Voronoi Tessellation over all points in the intial cell as depicted in Figure 3 and assigning the Voronoi polygons to a new cell containing all training samples in the computed OPTICS cluster. The area found through Voronoi Tessellation is then removed from the old geocell. The splitting is performed until convergence for each OPTICS parameter setting. In our work, we use three distinct OPTICS settings with values $\text{minsamples} = 8, 10, \text{ and } 15$ for the three respective rounds and xi parameters of 0.05, 0.025, and 0.015 for the same rounds. With each successive setting, the requirements defining a cluster are

Algorithm 1 Semantic Geocell Division Algorithm

```

Input: geocell boundaries  $g$ , training samples  $x$ ,  

OPTICS parameters  $p$ , minimum cell size MINSIZE.  

Initialize  $j = 1$ .  

repeat  

    Initialize  $C = \text{OPTICS}(p_j)$ .  

    for  $g_i$  in  $g$  do  

        Define  $x_i = \{x_j | x_j \in x \wedge x_j \in g_i\}$ .  

        repeat  

            Cluster  $c = C(x_i)$ .  

             $c_{max} = c_k$  where  $|x_{i,k}| \geq |x_{i,l}| \forall l$ .  

            if  $|c_{max}| > \text{MINSIZE}$  and  $|x \setminus x_{i,k}| > \text{MINSIZE}$  then  

                New cell  $g_{new} = \text{VORONOI}(x_{i,k})$ .  

                 $g_i = g_i \setminus g_{new}$ .  

                Assign  $x_i$  to cells  $i$  and  $new$ .  

            end if  

        until convergence  

    end for  

     $j = j + 1$   

until  $j$  is  $|p|$ 

```

thus relaxed to find clusters even in cells which are difficult to further divide.

Merging geocells according to administrative boundary hierarchies and dividing large cells based on our Semantic Geocell Division Algorithm results in geocells roughly balanced in size and which also preserve the semantics of cities, regions, countries, and the natural environment. By deploying our method to our training dataset, we compute the boundaries of a total of 2203 geocells used for our experiments.

4.2. Label Smoothing

By discretizing our image geolocalization problems via the help of our semantic geocells creation process, a trade-off is created between the granularity of geocells and predictive

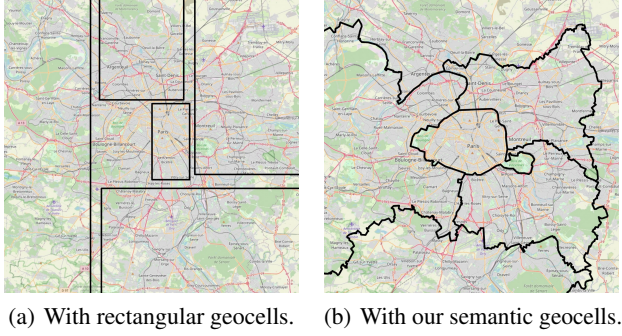


Figure 2. Île-de-France area around Paris, France, under different geocell creation specifications.



Figure 3. Voronoi tessellation applied in the process of geocell creation.

accuracy. The more granular the geocells are, the more precise a prediction can be but the classification problem becomes more difficult due to higher cardinality. To address this issue, we devise a loss function which penalizes based on the distance between the predicted geocell to the correct geocell. By smoothing the one-hot geocell classification label according to equation 1, we train our models in a much more data-efficient way as the parameters for multiple geocells are trained concurrently with each training example. The value of the smoothed one-hot label L_i for geocell i given the correct geocell c is given by

$$L_i = \exp(-[\text{Hav}(g_i, x_c) - \text{Hav}(g_c, x_c)] / 75) \quad (1)$$

where g_i are the centroid coordinates of the geocell polygon of cell i and x_c are the true coordinates of the example for which the label is computed. The constant of 75 acts as a temperature setting for the label smoothing which worked well in our experiments. $\text{Hav}(\cdot, \cdot)$ is the Haversine distance in kilometers defined as:

$$2r \arcsin \left(\sqrt{\sin^2 \left(\frac{\phi_2 - \phi_1}{2} \right) + \cos(\phi_1) \cos(\phi_2) \sin^2 \left(\frac{\lambda_2 - \lambda_1}{2} \right)} \right) \quad (2)$$

One advantage of using the Haversine distance between two points is that it respects the Earth’s spherical geometry, giving accurate estimates of the distance between two points. Figure 4 demonstrates the results of smoothing geocell labels which ideally results in lower geolocalization errors at the cost of slightly lower geocell prediction accuracy due to the added noise in the label.

By combining our semantic geocell design with label smoothing, we optimize for our model to spread probabilities across semantically similar *and* adjacent cells. Figure 5 shows the distribution of probabilities of our best model for a true location close to the sea in Jakobstad, Finland. Notably, our semantic geocell design and label smoothing results in our model placing high probabilities on semantically similar cells adjacent to the Gulf of Bothnia in Scandinavia.

4.3. Vision Transformer (CLIP)

The input image is encoded using a pre-trained vision transformer (Kolesnikov et al., 2021). We utilized a pretrained ViT-L/14 architecture and fine-tuning either the prediction heads or also unfreeze the last vision transformer layer. For model versions with multiple image inputs, we average the embeddings of all four images. Averaging the embeddings performed better during our experiments than combining the embeddings via multi-head attention or an additional transformer layer.

We were particularly interested in exploring the effect of the type of pretraining on downstream performance. We

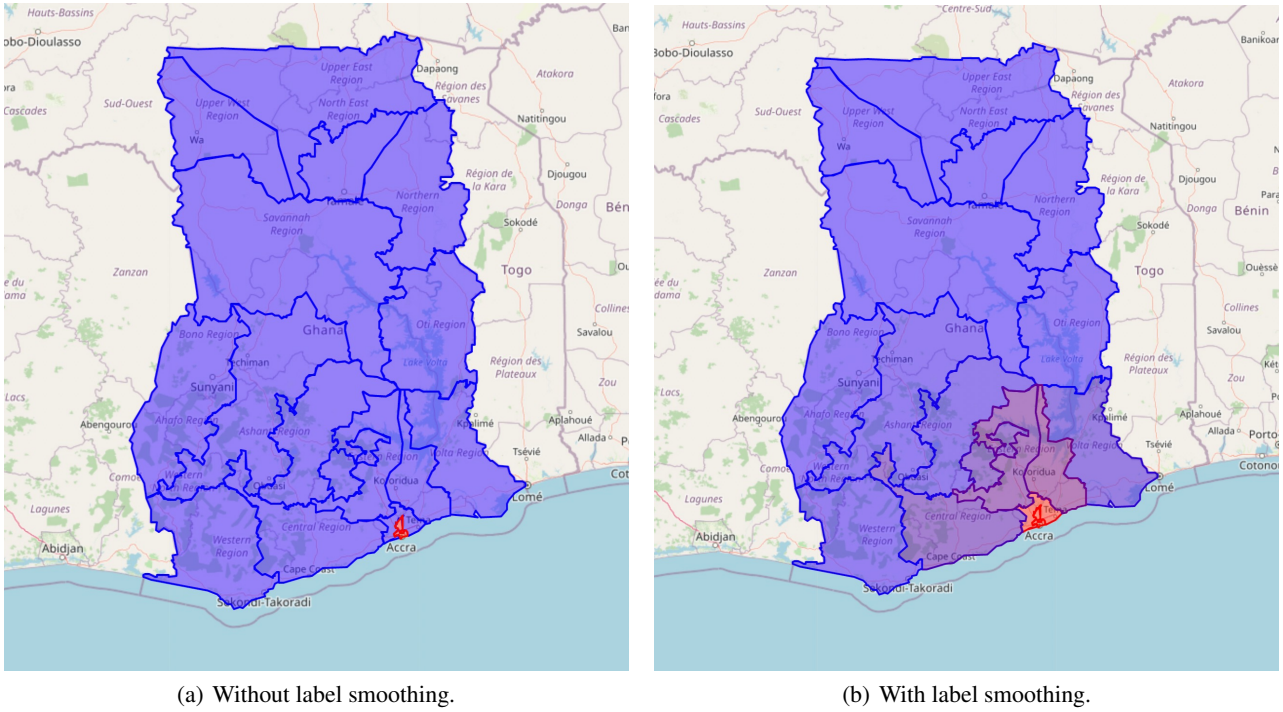


Figure 4. Impact of applying label smoothing over neighboring geocells for a location in Accra, Ghana.

compare a ViT-L/16 that was pre-trained ImageNet-21k with 14 million images (Deng et al., 2009) with CLIP ViT-L/14 which is a multi-modal model that utilized contrastive pre-training on a dataset of 400 million images and caption (Radford et al., 2021).

Based on our priors and commonly observed strategies by professional GeoGuessr players, there are a variety of relevant features for the image location task, e.g., vegetation, road markings, street signs, and architecture. We hypothesize that the multi-modal pre-training creates embeddings with a much deeper semantic understanding of the image, enabling it to learn such features. As we show later, the CLIP vision transformer gives a substantial improvement over a comparable ImageNet vision transformer and using attention maps, we can indeed show how this enables the model to learn these strategies in an interpretable way.

4.4. StreetCLIP Contrastive Pretraining

Inspired by the substantial improvement that we observed from using CLIP’s contrastive pre-training over the ImageNet pre-trained vision transformer, we explored designing a contrastive pre-training task that we could use to fine-tune our CLIP foundation model even before learning the geocell prediction head.

For that, we augment our Street View dataset with geographic, demographic, and geological auxiliary data. This

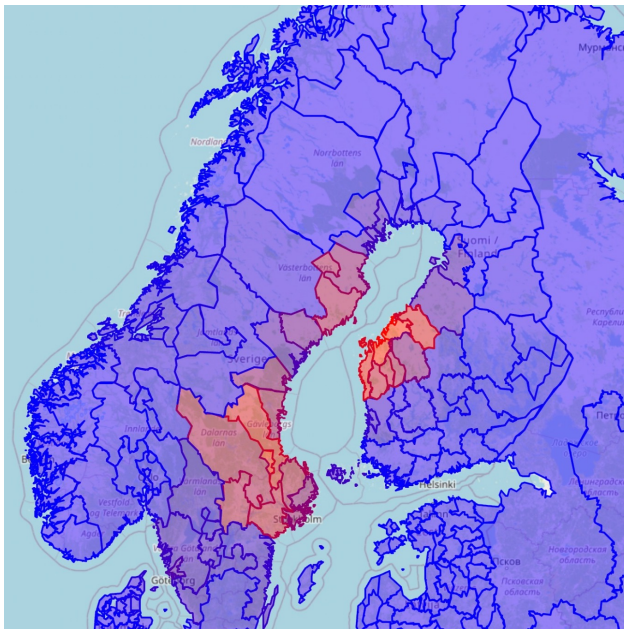


Figure 5. Distribution of probabilities over geocells for a true location in Jakobstad, Finland.

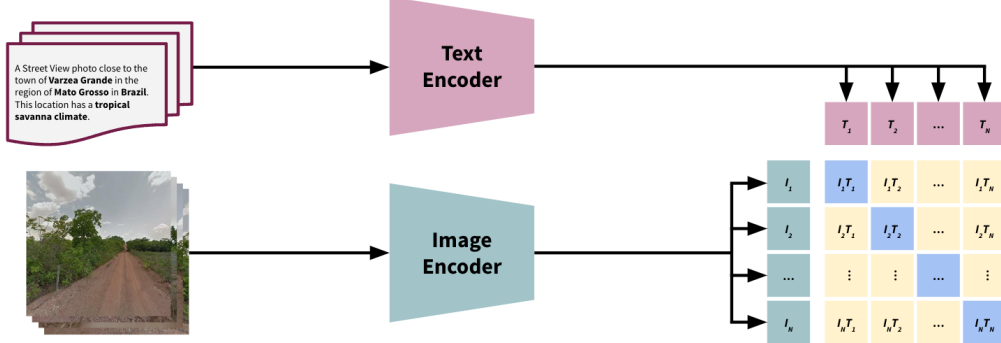


Figure 6. Contrastive pretraining of StreetCLIP (Haas et al., 2023) in an implicit multi-task setting using images from Varzea Grande, Mato Grosso, Brazil.

data is used to create randomized captions for each image using a rule-based system that samples components from different task categories and combines them in a randomized order. The probabilities for each category are adjusted based on priors. Some examples of categories & corresponding caption components include:

- Location: “A Street View photo in the region of Eastern Cape in South Africa.”
- Climate: “This location has a temperate oceanic climate.”
- Compass Direction: “This photo is facing north.”
- Season: “This photo was taken in December.”
- Traffic: “In this location, people drive on the left side of the road.”

This creates an implicit multi-task setting and ensures the model maintains rich representations of the data while adjusting to the distribution of Street View images and learning features that are relevant & correlated with geolocation.

4.5. Multi-task Learning

We also experiment with making our multi-task setup explicit by creating task-specific prediction heads for auxiliary climate variables, population density, elevation, and the month (season) of the year. As climate variables we include the Köppen-Geiger Climate Zone, the yearly average temperature and precipitation at the given location as well as the difference in temperature and precipitation between the month with the highest average value and the month with the lowest average value. The climate zone and season prediction tasks are posed as a classification problem while

the other six auxiliary tasks are formulated as a regression task.

In Hays & Efros (2014), the authors note that the “distribution of likely locations for an image provides huge amounts of additional meta-data for climate, average temperature for any day, vegetation index, elevation, population density, per capita income, average rainfall,” and more which can be leveraged for the task of geolocalization.

We unfreeze the last CLIP layer to allow for parameter sharing across tasks with the goal of observing a positive transfer from our auxiliary tasks to our geolocalization problem and to learn more general image representations which reduce the risk of overfitting to the training dataset. Our loss function weights the geolocalization tasks as much as all auxiliary tasks combined. A novel contribution of our work is that we use eight auxiliary prediction tasks instead of just two compared to prior research employing multi-task methods (Pramanick et al., 2022) with multi-task methods having shown impressive results across fields (Ruder, 2017).

4.6. ProtoNet Refinement

To further refine our model’s guesses within a geocell and to improve street and city-level performance, we perform intra-geocell refinement using ProtoNets (Snell et al., 2017). Instead of simply predicting the mean latitude and longitude of all points within a geocell as current state-of-the-art approaches such as Pramanick et al. (2022), we pose each cell’s intra-cell refinement as a separate few-shot classification task.

We again use the OPTICS clustering algorithm (Ankerst et al., 1999) with a minsample parameter of 3 and a xi parameter of 0.15 to cluster all points within a geocell and thus propose classes to learn in the intra-cell classification setting. Each cluster consisting of at least three training

examples forms a prototype and its representation is computed by averaging the embeddings of all images within the prototype. To compute the prototype embeddings, we use the same model as in our geocell prediction task but remove the prediction heads and freeze all weights. Figure 7 illustrates examples of refinement clusters found by the OPTICS algorithm in the Greater Los Angeles metropolitan area.

During inference, we first compute and average the new location’s embeddings. After our geocell classification model predicts, instead of predicting that cell’s centroid coordinates, we take the euclidian distance between the averaged image embeddings and all prototypes within the given geocell, selecting the prototype location with the smallest euclidian image embedding distance to the inference location as the final geolocalization prediction. The creation of intra-cell location prototypes allows our model to predict one of more than 11,000 distinct locations for a training dataset of 90,000 locations instead of just choosing from the 2,203 distinct geocell centroid coordinates, thus allowing for more precise decision making.

While guess refinement via protonets is in itself a novel idea, our work goes one step further by allow our ProtoNet refiner to optimize across cells. Instead of refining a geolocalization prediction in a single cell, our ProtoNet refiner optimizes across multiple cells which further increases performance. During inference, our geocell classification model outputs the top five predicted geocells as well as the model’s associated probabilities for these cells. The refinement model than picks the most likely location within each of the five proposed geocells after which a softmax is computed across the five euclidian image embedding distances yielded through ProtoNet refinement. We use a softmax with a temperature of 1.6 which was carefully tuned to balance probabilities across different geocells. Finally, these refinement probabilities are multiplied with the probabilities provided by the geocell classification model and the refinement location corresponding to the highest joint probability is chosen as the final geolocalization prediction.

5. Results

The results of our best-performing PIGEON model are listed in the bottom row of Tables 1 and 2. We achieve an astounding 91.96% Country Accuracy (based on political boundaries) and 40.36% of guesses are within 25 km of the correct location. Moreover, the median kilometer error is 44.35 km and the average GeoGuessr score is 4,525. In Table 3, we list the results of our multi-task models on our augmented dataset. Our results show that geographical, demographic, and geological features can be inferred from Street View images.

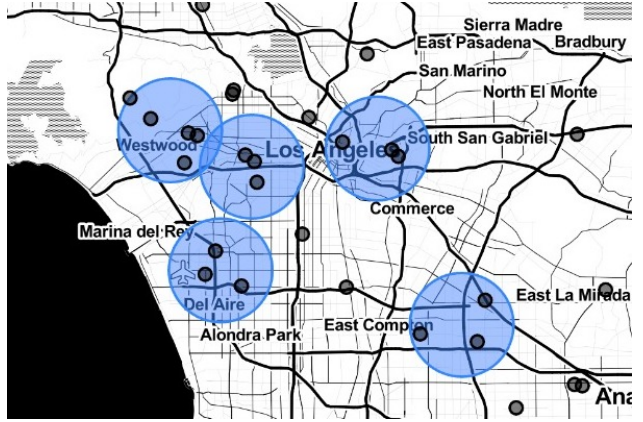


Figure 7. Visualized ProtoNet clusters in the Greater Los Angeles metropolitan area.

5.1. Ablation Studies on Geolocalization Accuracy

We perform a detailed ablation study for each of our methodological contributions as described in Section 4. We summarize our results in Table 1, displaying the percentage of our guesses that fall within a given kilometer radius from the actual location, using standard kilometer-based metrics in line with the literature (Pramanick et al., 2022). Furthermore, for each ablation, we calculate additional distance-based metrics in Table 2 that provide insights as to the performance of our modeling approach.

We have the following observations:

- Label Smoothing, Four-image Panorama, Multi-task Parameter Sharing, Semantic Geocells and CLIP Pre-training all significantly improve continent, country, and region-level metrics.
- On the other hand, ProtoNet Refinement has almost no effect on continent, country and region-level metrics, but significantly improves street-level accuracy from 1.32% to 4.84% as well as city level accuracy from 34.96% to 39.86%.
- Fine-tuning the last CLIP layer hurts model performance on its own, however, when performing multi-task training with the last CLIP layer as shared parameters, there is *positive transfer* and it *increases* performance. The multi-task training acts as a regularizer.
- When additionally performing the Contrastive Street-CLIP Pretraining then unfreezing the last CLIP layer again *hurts* performance. In particular, there is no positive transfer from the multi-task training anymore. Presumably, all of the benefits from multi-task supervision have already been captured from the implicitly multi-task StreetCLIP pretraining.

In Figure 8 we visualize the improvement of the best-performing PIGEON models over the simplest model using CLIP Base, showing how the performance gains are more palpable at finer granularities of distance compared to coarser distance metrics.

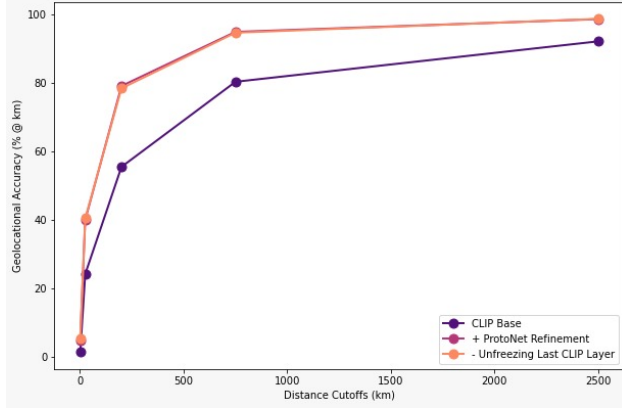


Figure 8. Geolocalization accuracy of our within distance-based standard metrics of km radii.

5.2. Contrastive Pretraining Results with StreetCLIP

The geolocation task is usually framed as a supervised learning problem. However, this has the major problem the models are very restricted to a specific task, e.g., the number of classes and the distribution of the training data. For example, our training dataset contains only Street View images during the day, whereas IM2GPS, a common benchmark dataset for geolocalization, contains a much wider distribution of images, e.g., images of the inside of buildings and images during the night. Moreover, both datasets have different non-overlapping sets of countries and differing definitions of countries, e.g., whether overseas territories like French Guiana or Guam are considered their own countries or not.

We have the hypothesis that StreetCLIP (Haas et al., 2023), through our Street View Multi-task Contrastive Pretraining, learns relevant strategies for geolocalization but keeps the general world knowledge from the original CLIP Pretraining. Thereby, it can generalize to countries it has never seen during our Street View Pretraining and is robust with regard to distribution shift.

We test our trained StreetCLIP model on the benchmark image geolocalization datasets IM2GPS and IM2GPS3k, which contain a much broader distribution of images than Street View. By generating an exhaustive list of 234 country captions, we perform a zero-shot linear probe of StreetCLIP to get country-level predictions which we then translate into coordinates. Table 4 presents our results. We compare against TransLocator Pramanick et al. (2022), the current

state-of-the-art on both of these datasets, and following their work, we report our performance on continent-level accuracy.

Whereas TransLocator was trained in a supervised manner on 4.72 million images, our model was trained in a semi-supervised manner on only 1 million Street View images. Surprisingly, despite the distribution shift, StreetCLIP outperforms the state-of-the-art on both benchmark datasets using just linear probing. In particular, StreetCLIP performs significantly better than CLIP which implies that there is a transfer of image geolocalization performance onto new distributions.

We conjecture that contrastive pretraining is performing *implicit meta-learning*. To further, confirm this hypothesis we investigated the performance of CLIP and StreetCLIP in countries that were not seen during StreetCLIP training (Haas et al., 2023). On the latest benchmark IM2GPS3K, StreetCLIP achieves an accuracy of 52.79% for countries not seen during unseen countries vs. 41.51% of accuracy for CLIP. An explanation for this surprising transfer is that the knowledge about these countries was already learned during the initial CLIP pertaining, e.g., the text encoder presumably has a good embedding of every country in the world. However, the StreetCLIP pretraining primes the model for the geolocalization tasks and unlocks additional knowledge from the original CLIP pretraining. Thereby, StreetCLIP can perform well on zero-shot transfer to new tasks (i.e., new countries) where our contrastive pretraining can be seen as a form of implicit meta-learning.

6. Analysis

We analyze our results in detail both through quantitative and qualitative evaluations. We confirmed the accuracy of our results by deploying our model in the GeoGuessr game, where our model consistently beats high-ranking human players, ranking in the Top 1,000 globally. We try to understand whether StreetCLIP is learning interpretable strategies by utilizing an explainability method. Furthermore, we analyze some of our underperforming guesses, and discuss the limitations of our work.

6.1. Quantitative Evaluation

6.1.1. COMPARISON WITH HUMAN PERFORMANCE

Using our Chrome extension (see Appendix D), we deploy PIGEON in online competitive GeoGuessr and aggregate the results of 298 rounds of the game mode Duel against human players of varying skill levels. We visualize the comparison of PIGEON with actual human in-game performance in Figure 9. Players are ranked into the following divisions by skill level: Bronze Division, Silver Division, Gold Division, Master Division, and Champion Division.

Table 1. Multi-step ablation study on our modeling approach to image geolocalization.

Method	Distance (%) @ km)				
	Street 1 km	City 25 km	Region 200 km	Country 750 km	Continent 2500 km
CLIP Base	1.28	24.08	55.38	80.20	92.00
+ Label Smoothing	0.92	24.18	59.04	82.84	92.76
+ Four-image Panorama	1.10	32.50	75.32	92.92	98.00
+ Fine-tuning Last CLIP Layer	1.10	32.74	75.14	93.00	97.98
+ Multi-task Parameter Sharing	1.18	33.22	75.42	93.42	98.16
+ Semantic Geocells	1.24	34.54	76.36	93.36	97.94
+ Contrastive CLIP Pretraining	1.32	34.96	78.48	94.82	98.48
+ ProtoNet Refinement	4.84	39.86	78.98	94.76	98.48
- Unfreezing Last CLIP Layer	5.36	40.36	78.28	94.52	98.56

Table 2. Results from the ablation study beyond the standard distance metrics (distance).

Method	Country Accuracy %	Mean km Error km	Median km Error km	GeoGuessr Score points
CLIP Base	72.12	990.0	148.0	3,890
+ Label Smoothing	74.74	877.4	131.1	3,986
+ Four-image Panorama	87.64	315.7	60.81	4,442
+ Fine-tuning Last CLIP Layer	87.90	312.7	61.81	4,442
+ Multi-task Parameter Sharing	87.96	299.9	60.63	4,454
+ Semantic Geocells	89.36	316.9	55.51	4,464
+ Contrastive CLIP Pretraining	91.14	251.9	50.01	4,522
+ ProtoNet Refinement	91.82	255.1	45.47	4,531
- Unfreezing Last CLIP Layer	91.96	251.6	44.35	4,525

Table 3. Results from the ablation study beyond the standard distance metrics (non-distance).

Method	Elevation Error m	Pop. Density Error people/km ²	Temp. Error °C	Precipitation Error mm/day	Month Accuracy %	Climate Zone Accuracy %
CLIP Base						
+ Label Smoothing						
+ Four-image Panorama						
+ Fine-tuning Last CLIP Layer						
+ Multi-task Parameter Sharing	141.7	1,094	1.37	14.48	45.74	74.10
+ Semantic Geocells	147.1	1,064	1.36	14.71	45.74	74.66
+ Contrastive CLIP Pretraining	132.8	1,072	1.18	12.82	50.64	75.76
+ ProtoNet Refinement						
- Unfreezing Last CLIP Layer	149.6	1,119	1.26	15.08	45.42	75.22

Table 4. Results from zero-shot probing with StreetCLIP (Haas et al., 2023) contrastive pretraining on out-of-distribution benchmark datasets.

Benchmark	Method	Distance % @ km
		Continent 2500 km
IM2GPS	TransLocator	86.70
	Zero-shot CLIP	86.08
	Zero-shot StreetCLIP	88.19
IM2GPS3K	TransLocator	80.10
	Zero-shot CLIP	77.28
	Zero-shot StreetCLIP	80.65

For reference, GeoGuessr has 30 million players worldwide, and the Master Division represents roughly the top 1% of players, whereas the Champion Division represents the Top 1000 players worldwide.

As we observe in Figure 9, PIGEON comfortably outperforms human performance. It even beats Champion Division players in median kilometer distance and, therefore, belongs to the Top 0.1% or Top 1000 players globally. Moreover, PIGEON is able to perform guesses almost instantly.

6.1.2. URBAN VS. RURAL

In order to elucidate the difficulty of different sub-distributions, we investigate whether a performance differential exists between urban and rural locations. Presumably, the density of relevant cues should be higher in Street View images from urban locations.

We bin our validation dataset into quintiles by population density and visualize PIGEON’s median kilometer error. In Figure 10, we observe that indeed higher population density correlates with better predictions. In particular, there is a sharp dropoff in the highest quintile compared to the other four quintiles. This confirms our hypothesis that there is a higher density of cues in urban locations.

6.2. Qualitative Evaluation

6.2.1. EXPLAINABILITY

One of our hypotheses in Section 4.3 was that the contrastive pre-training used by CLIP gives the model a deeper semantic understanding of scenes and thereby enables it to discover strategies that are interpretable by humans. Surprisingly, the model was able to learn strategies that are taught in online GeoGuessr guides without ever having been directly supervised to learn these strategies.

In order to visualize what patches of the image are considered relevant for a given caption, we visualize attention relevancy maps for our finetuned StreetCLIP model by im-

plementing the method from Generic Attention-model Explainability for Bi-Modal Transformers (Chefer et al., 2021).

In our experiments, we observed that this explainability method does not generalize well from a patch size of 32, as used in the official implementation, to our patch size of 14. Our hypothesis is that this is caused by the distribution of relevancy scores across patches having a lower entropy when the patch size is smaller. In order to resolve this issue, we modify the method by filtering out outliers and squaring relevancy scores. This significantly improved the interpretability of both regular CLIP and our StreetCLIP on smaller patch sizes and should be applicable beyond our project.

For the visualizations in Figure 11, we generated relevancy maps for an image from the validation dataset and the corresponding ground-truth caption, e.g. “This photo is located in Canada”. Indeed, the model pays attention to features that professional GeoGuessr players consider important, e.g., vegetation, road markings, utility posts, and signage. This makes the strong performance of the model explainable and could furthermore enable the discovery of new strategies that professional players have not yet discovered.

6.2.2. ERROR ANALYSIS

In spite of our model’s generally high accuracy of estimating image geolocations, there were several scenarios in which our model underperformed. By computing entropy for the probabilities of top predicted geocells for each location in our validation set, we managed to identify the images about the geolocation of which our model was the most uncertain. We visualize those cases in Figure 12.

The features of poorly classified images are aligned with our intuitions and prior literature about difficult settings for image geolocations. Figure 12 shows that images from tunnels, bodies of water, poorly illuminated areas, forest, indoor areas and soccer stadiums are amongst the imagery that is the most difficult to pinpoint geographically. This makes sense: without recognizable features directly pertaining to a specific geographical area, their classification is much more difficult when compared to images with features that clearly distinguish a given geography.

6.3. Limitations

Nevertheless, several limitations remain. Although PIGEON can successfully identify the vast majority of countries in which photos were taken, it still cannot be used at extremely precise levels (street-level) that are necessary for detailed geo-tagging. Moreover, the Street View images in our dataset were taken during daytime, raising doubts over the generalization of the model to images taken during nighttime. Further testing under different appearance variations

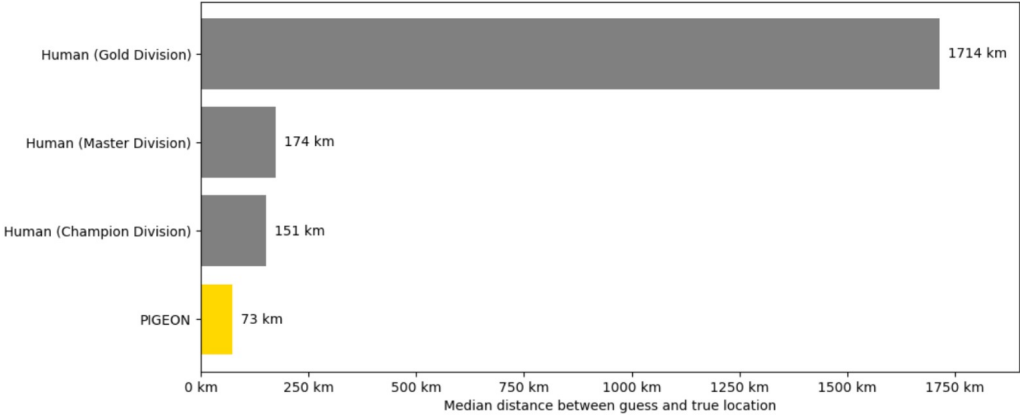


Figure 9. Comparison of the GeoGuessr in-game performance of PIGEON with the performance of actual online GeoGuessr players.

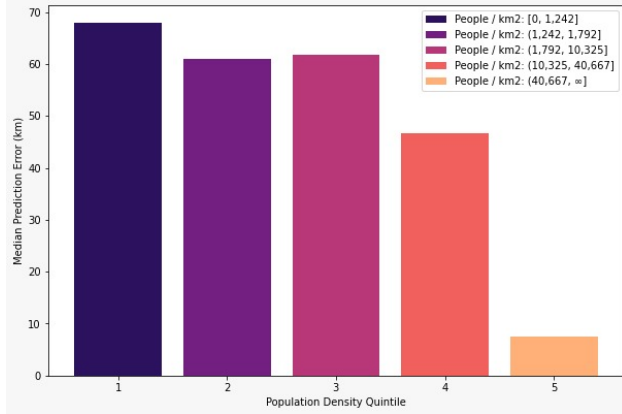


Figure 10. Median km error by population density quintile.

could provide insights into the robustness of PIGEON to different seasons, illuminations, weather, etc. Additionally, we recognize that some of our visualizations may be prone to cherry-picking, thus not being wholly representative of the underlying datasets.

7. Conclusion

Overall, PIGEON presents multiple novel improvements to multi-task image geolocalization while providing important insights and artifacts for related problems in fighting climate-change and urban and rural scene understanding. PIGEON achieves impressive results in planet-scale image geolocalization on Street View images, achieving a country accuracy of 91.96% on our held-out dataset and placing 40.36% of our guesses within 25 km of the target. Our model consistently beats human players in the game of GeoGuessr which samples data from the same distribution as introduced in our



(a) Attention attribution map for an image in Canada.



(b) Attention attribution map for an image in New Zealand.

Figure 11. Attention attribution maps for a sample of locations in our dataset.



(a) Image from a tunnel.



(b) Image from a body of water.



(c) Image from a dark area.



(d) Image from a forest.



(e) Image from an indoor area.



(f) Image from a soccer stadium.

Figure 12. Examples of images for which PIGEON was the most uncertain about the correct location.

novel dataset of 100,000 Street View locations.

The three major contributions of our work can be summarized as follows: we introduce a semantic geocell creation and splitting algorithm based on open-source data adaptable to any geospatial dataset. Second, we show the effectiveness of intra-geocell few-shot refinement via ProtoNets and the use clustering to generate potential prediction candidates. Finally, we make our pre-trained CLIP transformer model, StreetCLIP (Haas et al., 2023), publicly available for use by other researchers.

Finally, we show that contrastive pretraining is an effective meta-learning technique ideal for domain generalization and robustness to distribution shifts. One of the most important results of our work is achieving state-of-the-art performance on the IM2GPS and IM2GPS3k image geolocation benchmark datasets which are strongly out-of-distribution compared to our Street View dataset used for the pre-training of StreetCLIP. Most notably, the state-of-the art performance achieved is in zero-shot, shining light on the potential of StreetCLIP to help solve problems in many other domains.

8. Future Work

8.1. Potential Extensions

Going forward, several extensions can be made to make image geolocation more precise. Future models can detect text included in images to leverage linguistic information for predictions, with textual data having previously been suggested as a potential feature aiding geolocation (Arbinger et al., 2022). Instead of being constrained to street-level imagery, cross-view approaches could be employed, such as synthesizing satellite imagery with Street View (Toker et al., 2021). Although we propose novel semantic geocells, our experiments are constrained to one granularity of geocells; in the future, various granularities of geocells can be tested to find the optimal geocell sizes. Ideally, future image geolocation models would be robust to appearance changes, which bring up the need for incorporating changes over the years, requiring datasets of images over an extended period of time over a year (Ali-bey et al., 2022). In a multi-task setting, determining the optimal number of tasks is likely to be a priority. Additionally, image segmentation and concept influence could be used for further location prediction interpretability, and fusions between images to get information about the entire four-image panorama and not just individual images. In the long term, future work could go beyond Street View, with the models able to geolocate any photo taken anywhere in the world at fine-grained granularity. To that end, future experiments in CLIP-based zero-shot settings should go beyond just the continent-level accuracy.

Some additional extensions we thought of exploring in this project, but did not end up pursuing, include using knowledge graphs, using road networks and compass directions for intra-geocell refinement, as well as adding an urban/rural scene recognition task to the multi-task setting.

8.2. Social Impact

The results we achieved have vast social impact potential. By predicting climate based on images, we could be able to assess the risk to the consequences of climate change. This is why we decided to augment our data specifically with the Köppen-Geiger climate classification system given its emphasis on the geospatial understanding of the impacts of climate change (Beck et al., 2018). Image geolocalization can also be used for applications in autonomous driving (Wilson et al., 2021), in war zones (such as during the Russian invasion of Ukraine), for attributing location to archival images, helping historical research, as well as in promoting geography education through gamified e-learning (Girgin, 2017).

Even with the potential benefits to humans, image geolocalization nevertheless has to deal with various ethical issues. Some actors posting images might not want their images to be geolocalized, leading to questions about the fragility of privacy protections. Furthermore, accurate image geolocalization systems could be used by governments for citizen surveillance, posing a threat to individual freedoms.

References

- Ali-bey, A., Chaib-draa, B., and Giguère, P. GSV-Cities: Toward appropriate supervised visual place recognition. *Neurocomputing*, 513:194–203, 2022. ISSN 0925-2312. doi: <https://doi.org/10.1016/j.neucom.2022.09.127>. URL <https://www.sciencedirect.com/science/article/pii/S0925231222012188>.
- Ankerst, M., Breunig, M. M., Kriegel, H.-P., and Sander, J. OPTICS: Ordering Points to Identify the Clustering Structure. In *Proceedings of the 1999 ACM SIGMOD International Conference on Management of Data, SIGMOD '99*, pp. 49–60, New York, NY, USA, 1999. Association for Computing Machinery. ISBN 1581130848. doi: 10.1145/304182.304187. URL <https://doi.org/10.1145/304182.304187>.
- Arbinger, C., Bullin, M., and Henrich, A. Exploiting geodata to improve image recognition with deep learning. In *Companion Proceedings of the Web Conference 2022, WWW '22*, pp. 648–655, New York, NY, USA, 2022. Association for Computing Machinery. ISBN 9781450391306. doi: 10.1145/3487553.3524645. URL <https://doi.org/10.1145/3487553.3524645>.
- Ardeshir, S., Zamir, A. R., Torroella, A., and Shah, M. GIS-Assisted Object Detection and Geospatial Localization. In Fleet, D., Pajdla, T., Schiele, B., and Tuytelaars, T. (eds.), *Computer Vision – ECCV 2014*, pp. 602–617, Cham, 2014. Springer International Publishing. ISBN 978-3-319-10599-4.
- Baatz, G., Saurer, O., Köser, K., and Pollefey, M. Large Scale Visual Geo-Localization of Images in Mountainous Terrain. In Fitzgibbon, A., Lazebnik, S., Perona, P., Sato, Y., and Schmid, C. (eds.), *Computer Vision – ECCV 2012*, pp. 517–530, Berlin, Heidelberg, 2012. Springer Berlin Heidelberg. ISBN 978-3-642-33709-3.
- Beck, H. E., Zimmermann, N. E., McVicar, T. R., Vergopolan, N., Berg, A., and Wood, E. F. Present and future köppen-geiger climate classification maps at 1-km resolution. *Scientific Data*, 5(1):180214, Oct 2018. ISSN 2052-4463. doi: 10.1038/sdata.2018.214. URL <https://doi.org/10.1038/sdata.2018.214>.
- Bertoni, G., Masone, C., and Caputo, B. Rethinking Visual Geo-localization for Large-Scale Applications, 2022a. URL <https://arxiv.org/abs/2204.02287>.
- Bertoni, G., Mereu, R., Trivigno, G., Masone, C., Csurka, G., Sattler, T., and Caputo, B. Deep Visual Geo-localization Benchmark, 2022b. URL <https://arxiv.org/abs/2204.03444>.

- Bingel, J. and Søgaard, A. Identifying beneficial task relations for multi-task learning in deep neural networks, 2017. URL <https://arxiv.org/abs/1702.08303>.
- Browning, K. Siberia or Japan? Expert Google Maps Players Can Tell at a Glimpse., 2022. URL <https://www.nytimes.com/2022/07/07/business/geoguessr-google-maps.html>.
- Cao, L., Smith, J. R., Wen, Z., Yin, Z., Jin, X., and Han, J. BlueFinder: Estimate Where a Beach Photo Was Taken. In *Proceedings of the 21st International Conference on World Wide Web*, WWW '12 Companion, pp. 469–470, New York, NY, USA, 2012. Association for Computing Machinery. ISBN 9781450312301. doi: 10.1145/2187980.2188081. URL <https://doi.org/10.1145/2187980.2188081>.
- Cassens, L. AI learns GeoGuessr and plays against pro!, 2022. URL <https://www.youtube.com/watch?v=0k-SJgv-laM>.
- Chefer, H., Gur, S., and Wolf, L. Generic attention-model explainability for interpreting bi-modal and encoder-decoder transformers, 2021. URL <https://arxiv.org/abs/2103.15679>.
- Crandall, D., Backstrom, L., Huttenlocher, D., and Kleinberg, J. Mapping the World's Photos. In *WWW '09: Proceedings of the 18th International Conference on World Wide Web*, pp. 761–880, 2009.
- de Brebisson, A., Simon, E., Auvolat, A., Vincent, P., and Bengio, Y. Artificial Neural Networks Applied to Taxi Destination Prediction, 2015. URL <https://arxiv.org/abs/1508.00021>.
- de Fontnouvelle, V. GeoGuessrBot: Predicting the Location of Any Street View Image, 2021. URL <https://vdefont.github.io/2021/06/20/geoguessr.html>.
- Deng, J., Dong, W., Socher, R., Li, L.-J., Li, K., and Fei-Fei, L. Imagenet: A large-scale hierarchical image database. In *2009 IEEE Conference on Computer Vision and Pattern Recognition*, pp. 248–255, 2009. doi: 10.1109/CVPR.2009.5206848.
- Fick, S. E. and Hijmans, R. J. WorldClim 2: new 1-km spatial resolution climate surfaces for global land areas. *International Journal of Climatology*, 37(12): 4302–4315, 2017. doi: <https://doi.org/10.1002/joc.5086>. URL <https://rmets.onlinelibrary.wiley.com/doi/10.1002/joc.5086>.
- GADM. GADM Version 4.1, 2022. URL <https://gadm.org/about.html>.
- Gebru, T., Krause, J., Wang, Y., Chen, D., Deng, J., Aiden, E. L., and Fei-Fei, L. Using deep learning and Google Street View to estimate the demographic makeup of neighborhoods across the United States. *Proceedings of the National Academy of Sciences*, 114(50):13108–13113, 2017. doi: 10.1073/pnas.1700035114. URL <https://www.pnas.org/doi/abs/10.1073/pnas.1700035114>.
- Girgin, M. Use of Games in Education: GeoGuessr in Geography Course. *International Technology and Education Journal*, 2017.
- Haas, L., Alberti, S., and Skreta, M. Learning generalized zero-shot learners for open-domain image geolocalization, 2023.
- Hays, J. and Efros, A. A. IM2GPS: estimating geographic information from a single image. In *Proceedings of the IEEE Conf. on Computer Vision and Pattern Recognition (CVPR)*, 2008.
- Hays, J. and Efros, A. A. *Multimodal Location Estimation of Videos and Images*, chapter Large-Scale Image Geolocalization. Springer, 2014.
- Howard, A. G., Zhu, M., Chen, B., Kalenichenko, D., Wang, W., Weyand, T., Andreetto, M., and Adam, H. Mobilenets: Efficient convolutional neural networks for mobile vision applications, 2017. URL <https://arxiv.org/abs/1704.04861>.
- Izbicki, M., Papalexakis, E. E., and Tsotras, V. J. Exploiting the Earth's Spherical Geometry to Geolocate Images. In *Joint European Conference on Machine Learning and Knowledge Discovery in Databases*, pp. 3–19, 2019.
- Kolesnikov, A., Dosovitskiy, A., Weissenborn, D., Heigold, G., Uszkoreit, J., Beyer, L., Minderer, M., Dehghani, M., Houlsby, N., Gelly, S., Unterthiner, T., and Zhai, X. An image is worth 16x16 words: Transformers for image recognition at scale. 2021.
- Kordopatis-Zilos, G., Galopoulos, P., Papadopoulos, S., and Kompatsiaris, I. Leveraging EfficientNet and Contrastive Learning for Accurate Global-scale Location Estimation, 2021. URL <https://arxiv.org/abs/2105.07645>.
- Krizhevsky, A., Sutskever, I., and Hinton, G. E. ImageNet Classification with Deep Convolutional Neural Networks. In Pereira, F., Burges, C., Bottou, L., and Weinberger, K. (eds.), *Advances in Neural Information Processing Systems*, volume 25. Curran Associates, Inc., 2012. URL <https://proceedings.neurips.cc/paper/2012/file/c399862d3b9d6b76c8436e924a68c45b-Paper.pdf>.

- Li, W. and Hsu, C.-Y. Geoai for large-scale image analysis and machine vision: Recent progress of artificial intelligence in geography. *ISPRS International Journal of Geo-Information*, 11(7), 2022. ISSN 2220-9964. doi: 10.3390/ijgi11070385. URL <https://www.mdpi.com/2220-9964/11/7/385>.
- Lin, T.-Y., Belongie, S., and Hays, J. Cross-View Image Geolocalization. In *2013 IEEE Conference on Computer Vision and Pattern Recognition*, pp. 891–898, 2013. doi: 10.1109/CVPR.2013.120.
- Luo, G., Biamby, G., Darrell, T., Fried, D., and Rohrbach, A. G'3: Geolocation via Guidebook Grounding, 2022. URL <https://arxiv.org/abs/2211.15521>.
- Mai, G., Janowicz, K., Hu, Y., Gao, S., Yan, B., Zhu, R., Cai, L., and Lao, N. A review of location encoding for geoai: methods and applications. *International Journal of Geographical Information Science*, 36(4):639–673, 2022. doi: 10.1080/13658816.2021.2004602. URL <https://doi.org/10.1080/13658816.2021.2004602>.
- Masone, C. and Caputo, B. A survey on deep visual place recognition. *IEEE Access*, 9:19516–19547, 2021. doi: 10.1109/ACCESS.2021.3054937.
- Mayer, K., Haas, L., Huang, T., Bernabé-Moreno, J., Rajagopal, R., and Fischer, M. Estimating building energy efficiency from street view imagery, aerial imagery, and land surface temperature data, 2022. URL <https://arxiv.org/abs/2206.02270>.
- Müller-Budack, E., Pustu-Iren, K., and Ewerth, R. Geolocation Estimation of Photos using a Hierarchical Model and Scene Classification. In *Proceedings of the European Conference on Computer Vision (ECCV)*, pp. 563–579, 2018.
- Pramanick, S., Nowara, E. M., Gleason, J., Castillo, C. D., and Chellappa, R. Where in the World is this Image? Transformer-based Geo-localization in the Wild, 2022. URL <https://arxiv.org/abs/2204.13861>.
- Radford, A., Kim, J. W., Hallacy, C., Ramesh, A., Goh, G., Agarwal, S., Sastry, G., Askell, A., Mishkin, P., Clark, J., Krueger, G., and Sutskever, I. Learning Transferable Visual Models From Natural Language Supervision. *CoRR*, abs/2103.00020, 2021. URL <https://arxiv.org/abs/2103.00020>.
- Raghuram, M., Unterthiner, T., Kornblith, S., Zhang, C., and Dosovitskiy, A. Do Vision Transformers See Like Convolutional Neural Networks? *CoRR*, abs/2108.08810, 2021. URL <https://arxiv.org/abs/2108.08810>.
- Ranjan, R., Patel, V. M., and Chellappa, R. HyperFace: A Deep Multi-task Learning Framework for Face Detection, Landmark Localization, Pose Estimation, and Gender Recognition. *CoRR*, abs/1603.01249, 2016. URL <http://arxiv.org/abs/1603.01249>.
- Ruder, S. An Overview of Multi-Task Learning in Deep Neural Networks. *CoRR*, abs/1706.05098, 2017. URL <http://arxiv.org/abs/1706.05098>.
- Rußwurm, M., Wang, S., Körner, M., and Lobell, D. Meta-Learning for Few-Shot Land Cover Classification, 2020. URL <https://arxiv.org/abs/2004.13390>.
- Saurer, O., Baatz, G., Köser, K., Ladický, L., and Pollefeys, M. Image based geo-localization in the alps. *International Journal of Computer Vision*, 116(3):213–225, Feb 2016. ISSN 1573-1405. doi: 10.1007/s11263-015-0830-0. URL <https://doi.org/10.1007/s11263-015-0830-0>.
- Seo, P. H., Weyand, T., Sim, J., and Han, B. CPlaNet: Enhancing Image Geolocalization by Combinatorial Partitioning of Maps, 2018. URL <https://arxiv.org/abs/1808.02130>.
- Seymour, Z., Sikka, K., Chiu, H., Samarasakera, S., and Kumar, R. Semantically-Aware Attentive Neural Embeddings for Image-based Visual Localization. *CoRR*, abs/1812.03402, 2018. URL <http://arxiv.org/abs/1812.03402>.
- Snell, J., Swersky, K., and Zemel, R. S. Prototypical Networks for Few-shot Learning. *CoRR*, abs/1703.05175, 2017. URL <http://arxiv.org/abs/1703.05175>.
- Suresh, S., Chodosh, N., and Abello, M. DeepGeo: Photo Localization with Deep Neural Network, 2018. URL <https://arxiv.org/abs/1810.03077>.
- Theiner, J., Müller-Budack, E., and Ewerth, R. Interpretable Semantic Photo Geolocation. In *2022 IEEE/CVF Winter Conference on Applications of Computer Vision (WACV)*, pp. 1474–1484, 2022. doi: 10.1109/WACV51458.2022.00154.
- Toker, A., Zhou, Q., Maximov, M., and Leal-Taixé, L. Coming Down to Earth: Satellite-to-Street View Synthesis for Geo-Localization. In *2021 IEEE/CVF Conference on Computer Vision and Pattern Recognition (CVPR)*, pp. 6484–6493, Los Alamitos, CA, USA, jun 2021. IEEE Computer Society. doi: 10.1109/CVPR46437.2021.00642. URL <https://doi.ieee.org/10.1109/CVPR46437.2021.00642>.

- Tomešek, J., Čadík, M., and Brejcha, J. CrossLocate: Cross-Modal Large-Scale Visual Geo-Localization in Natural Environments Using Rendered Modalities. In *Proceedings of the IEEE/CVF Winter Conference on Applications of Computer Vision (WACV)*, pp. 3174–3183, January 2022.
- Tzeng, E., Zhai, A., Clements, M., Townshend, R., and Zakhori, A. User-Driven Geolocation of Untagged Desert Imagery Using Digital Elevation Models. In *2013 IEEE Conference on Computer Vision and Pattern Recognition Workshops*, pp. 237–244, 2013. doi: 10.1109/CVPRW.2013.42.
- Vaswani, A., Shazeer, N., Parmar, N., Uszkoreit, J., Jones, L., Gomez, A. N., Kaiser, L., and Polosukhin, I. Attention Is All You Need, 2017. URL <https://arxiv.org/abs/1706.03762>.
- Vo, N., Jacobs, N., and Hays, J. Revisiting IM2GPS in the Deep Learning Era, 2017. URL <https://arxiv.org/abs/1705.04838>.
- Weyand, T., Kostrikov, I., and Philbin, J. PlaNet - Photo Geolocation with Convolutional Neural Networks. In *Computer Vision – ECCV 2016*, pp. 37–55. Springer International Publishing, 2016. doi: 10.1007/978-3-319-46484-8_3. URL https://doi.org/10.1007%2F978-3-319-46484-8_3.
- Weyand, T., Araujo, A., Cao, B., and Sim, J. Google Landmarks Dataset v2 – A Large-Scale Benchmark for Instance-Level Recognition and Retrieval, 2020. URL <https://arxiv.org/abs/2004.01804>.
- Wilson, D., Zhang, X., Sultani, W., and Wshah, S. Visual and object geo-localization: A comprehensive survey. *CoRR*, abs/2112.15202, 2021. URL <https://arxiv.org/abs/2112.15202>.
- Wu, M. and Huang, Q. Im2city: Image geo-localization via multi-modal learning. In *Proceedings of the 5th ACM SIGSPATIAL International Workshop on AI for Geographic Knowledge Discovery, GeoAI ’22*, pp. 50–61, New York, NY, USA, 2022. Association for Computing Machinery. ISBN 9781450395328. doi: 10.1145/3557918.3565868. URL <https://doi.org/10.1145/3557918.3565868>.
- Yang, H., Lu, X., and Zhu, Y. Cross-view Geo-localization with Layer-to-Layer Transformer. In Ranzato, M., Beygelzimer, A., Dauphin, Y., Liang, P., and Vaughan, J. W. (eds.), *Advances in Neural Information Processing Systems*, volume 34, pp. 29009–29020. Curran Associates, Inc., 2021. URL <https://proceedings.neurips.cc/paper/2021/file/f31b20466ae89669f9741e047487eb37-Paper.pdf>.
- Zamir, A. R. and Shah, M. Accurate image localization based on google maps street view. In Daniilidis, K., Maragos, P., and Paragios, N. (eds.), *Computer Vision – ECCV 2010*, pp. 255–268, Berlin, Heidelberg, 2010. Springer Berlin Heidelberg. ISBN 978-3-642-15561-1.
- Zamir, A. R. and Shah, M. Image geo-localization based on multiplenearest neighbor feature matching using generalized graphs. *IEEE Transactions on Pattern Analysis and Machine Intelligence*, 36(8):1546–1558, 2014. doi: 10.1109/TPAMI.2014.2299799.
- Zhu, S., Shah, M., and Chen, C. TransGeo: Transformer Is All You Need for Cross-view Image Geolocation, 2022. URL <https://arxiv.org/abs/2204.00097>.

In this Appendix, we provide additional information that describes our work in further detail.

In Section A, we list our data sources and visualize the data used for augmenting our dataset. In Section B, we provide details regarding the process of obtaining our images from the Street View API. In Section C, we discuss the background of the GeoGuessr game that is relevant for understanding this project. In Section D, we describe a Chrome Extension we built to play GeoGuessr by deploying our model online, allowing us to compare our results to human performance. In Section E, we describe the technical details about the infrastructure used for running our models as well as the hyperparameters used during model training.

A. Data Specification for Dataset Augmentation

A.1. Country Area Polygons

We obtain data on country areas from the Database of Global Administrative Areas (GADM) (GADM, 2022), with the data available [here](#). Additionally, we obtain data on several granularities of political boundaries of administrative areas, with the data available [here](#) and [here](#).

A.2. Köppen-Geiger Climate Zones

We obtain data on global climate zones through the Köppen-Geiger climate classification system (Beck et al., 2018), with the data available [here](#).

Our planet-scale climate zone data is visualized in Figure 13.

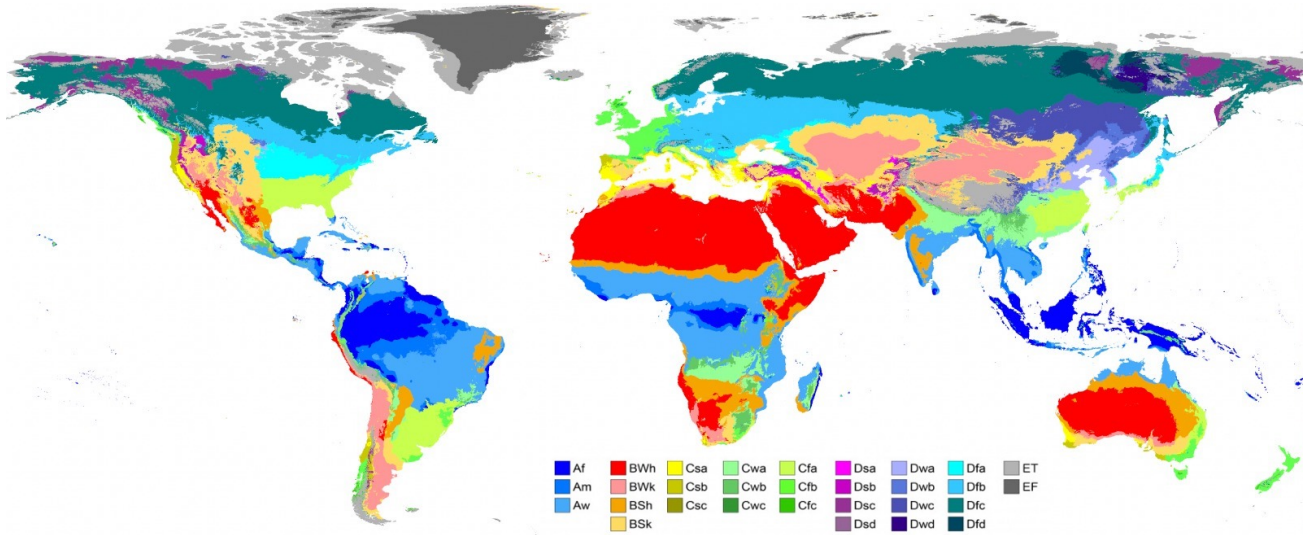


Figure 13. Map of planet-scale Köppen-Geiger climate zones in our dataset. Adapted from Beck et al. (2018).

A.3. Elevation

We obtain data on elevation through the United States Geological Survey's Earth Resources Observation and Science (EROS) Center, with the data available [here](#). As elevation data was missing for several locations in our dataset, we further augmented our data with missing values from parts of Alaska and parts of Europe, with the data for Alaska available [here](#) and the data for Europe available [here](#).

Our planet-scale elevation data is visualized in Figure 14.

A.4. GHSL Population Density

We obtain data on population density through the Global Human Settlement Layer (GHSL), with the data available [here](#).



Figure 14. Map of planet-scale elevation in our validation dataset.

Our planet-scale population density data is visualized in Figure 15.

A.5. WorldClim 2 Temperature and Precipitation

We obtain data on average temperature, temperature difference, average precipitation, and precipitation difference through WorldClim 2 (Fick & Hijmans, 2017), with the data available [here](#).

Our planet-scale average temperature is visualized in Figure 16. Our planet-scale temperature difference is visualized in Figure 17. Our planet-scale average precipitation is visualized in Figure 18. Our planet-scale precipitation difference is visualized in Figure 19.

A.6. Location of Country Capitals

We obtain data on the locations of country capitals used for refining our zero-shot StreetCLIP predictions through Kaggle, with the data available [here](#).

A.7. Alpha-2 Country Codes

We obtain our ISO 3166-2 alpha-2 country codes used for matching country codes generated through the Street View API with country names through Kaggle, with the data available [here](#).

A.8. Driving Side of the Road

We obtain our driving side of the road data through WorldStandards, with the data available [here](#).

B. Querying Street View API

After signing an NDA with Erland Ranvinge, the Chief Technology Officer of GeoGuessr, we obtained a list of exactly one million locations that actually appear in the Competitive Duels mode of GeoGuessr. From that list, we randomly sampled



Figure 15. Map of planet-scale population density in our validation dataset.

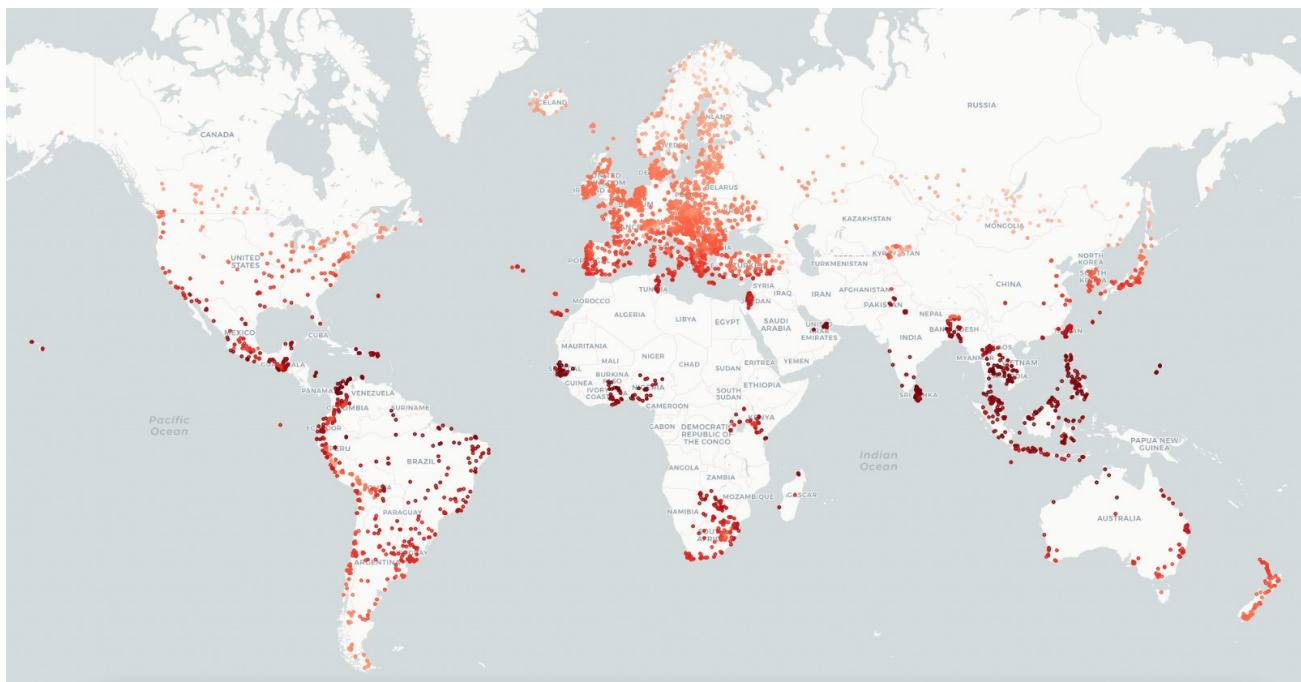


Figure 16. Map of planet-scale average temperature in our validation dataset.

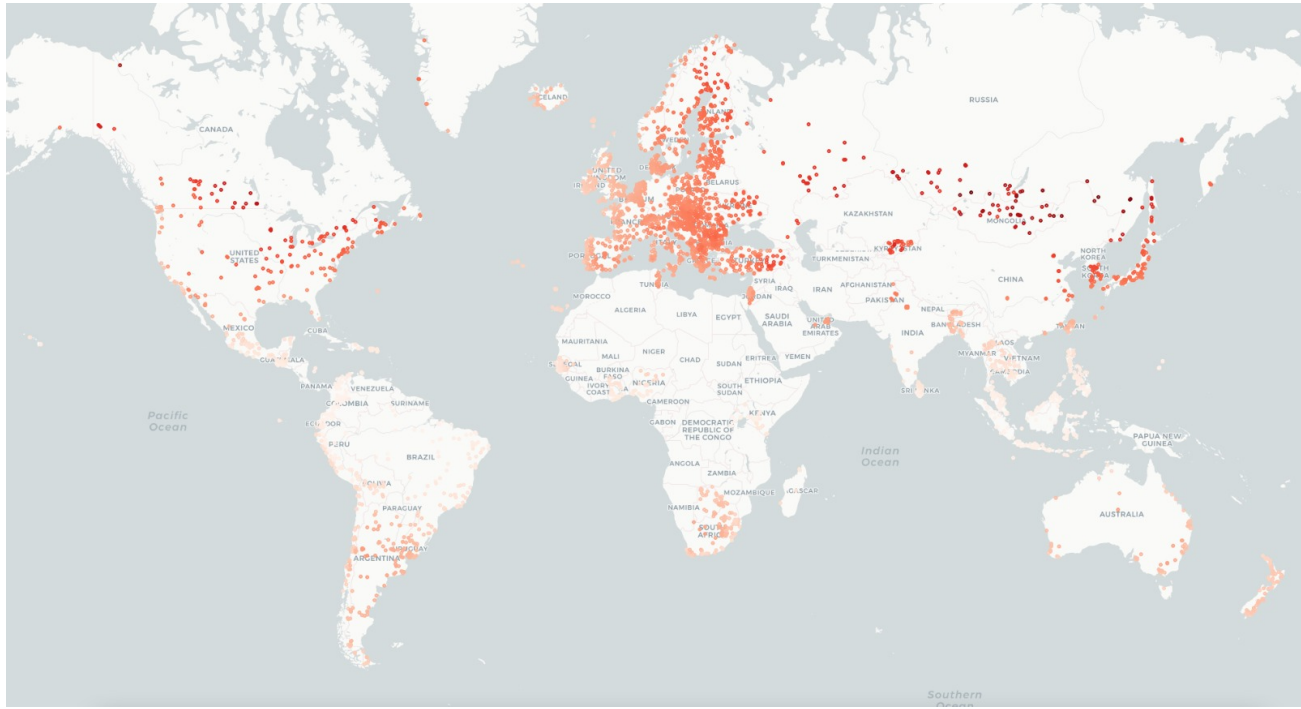


Figure 17. Map of planet-scale temperature difference in our validation dataset.



Figure 18. Map of planet-scale average precipitation in our validation dataset.



Figure 19. Map of planet-scale precipitation difference in our validation dataset.

100,000 locations, or 10% of the dataset, maintaining the distribution of countries representative of the larger dataset as visualized in Figure 20.

It should be emphasized, however, that while the distribution is representative of the broader distribution of locations in Google Street View, the Google Street View distribution itself cannot be thought of as a uniform global distribution, as visualized in Figure 21.

To obtain the actual images from our dataset, we queried the [Street View API](#) using the Google Cloud Platform Education Grants generously supplied to us by Google with the help of Dan Russell.

B.1. Metadata

We first queried the Street View API for the location metadata by supplying a `pano_id`, or an id pertaining to each location, with each request. That way, we were able to verify whether Street View images actually existed in this location and which month and year a given image was taken. For each unavailable image, we sampled a random location from the same country to maintain the prior distribution. Each metadata request was free of charge.

B.2. Images

Subsequently, we proceeded to download images from each location. Aside from the `pano_id`, we specified additional parameters specific to Street View image downloads. We chose the image size `size` to be 640×640 pixels, or the largest available size. For each location, we generated a random `heading`, or compass direction, between 0 and 359, and added 90 degrees to each subsequent picture for that location to come up with a full panorama. Subsequently, we chose a field of view, `fov` of 92, allowing us to retain all of the image's information even after cropping the watermarks. We picked our `source` parameter as `outdoor` to be limited to outdoor images, however a small portion of images was still from indoors, as Figure 12 shows, emphasizing mislabeling on Google's side. For the remaining parameters, we set the default values to 0 for `pitch`, 50 for `radius`, and `true` for `return_error_code`. All in all, this allowed us to download images consistently for each location in our dataset.

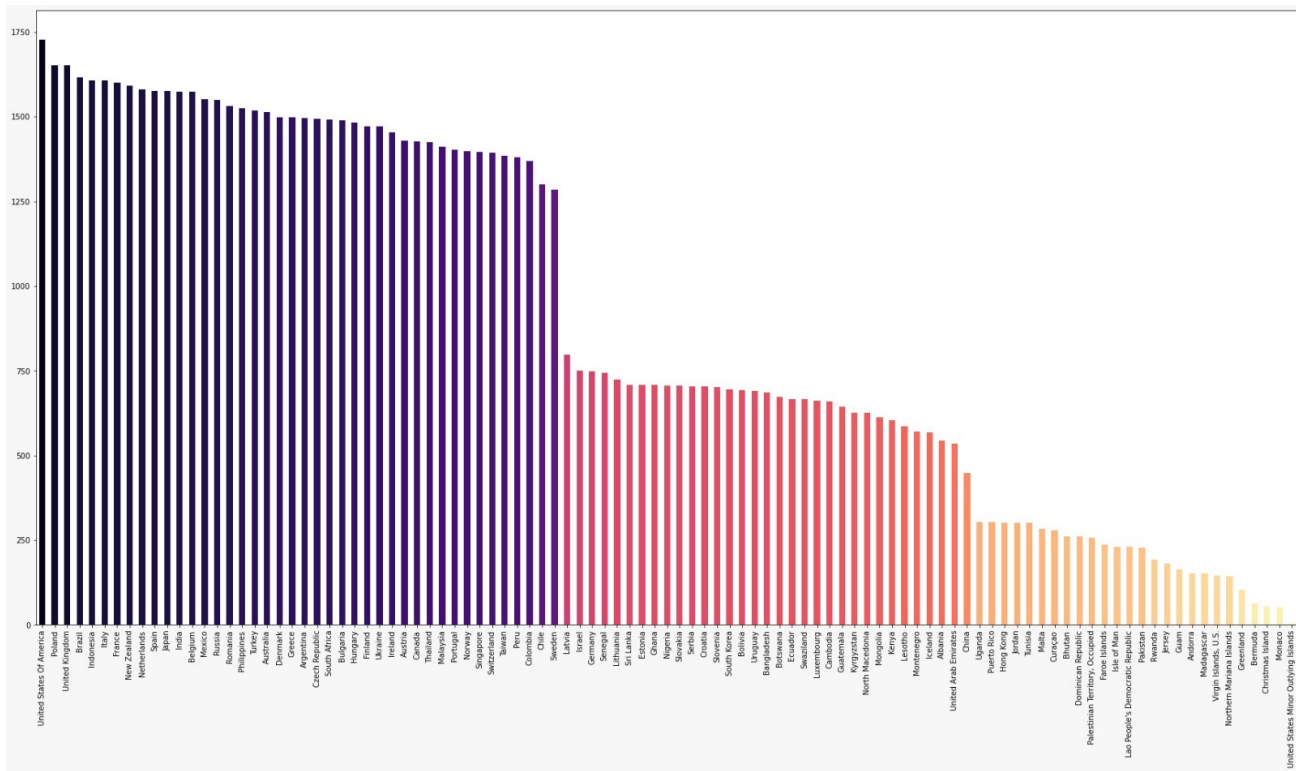


Figure 20. Distribution of countries in our training set, colored by the tiers of frequency.

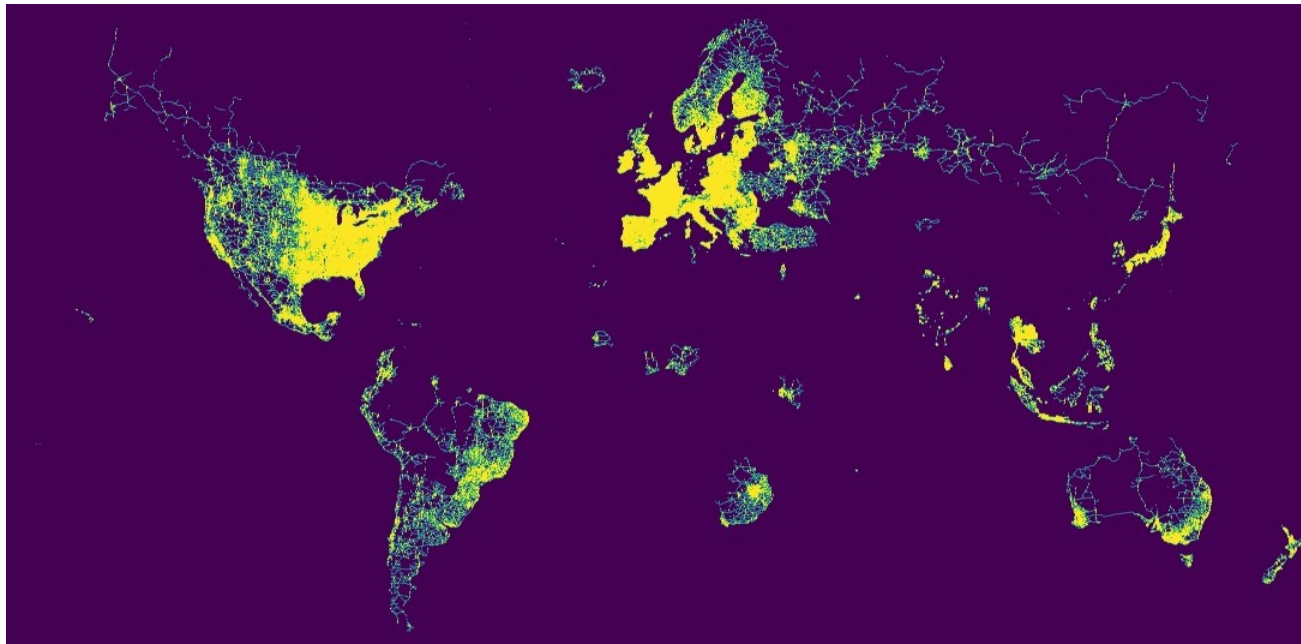


Figure 21. Map of planet-scale Google Street View coverage. Courtesy of [Lion Cassens](#).

C. Background on GeoGuessr

GeoGuessr is an online game founded in Sweden in 2013. Upon starting the game, the user is placed in a location supplied by Google Street View and needs to guess where that location is in the world by placing a guess on the map. The game can be played in both single- and multi-player modes on maps that are both GeoGuessr-provided as well as user-generated. When playing with others, users can play both with their friends as well as with random opponents on the Internet. We decided to focus PIGEON on the Competitive Duels mode, whereby the user directly competes with an opponent and thus must not only place guesses accurately but also more accurately than the opponent. Each guess is translated into a GeoGuessr score, the function of which we re-engineered as outlined in Equation 3:

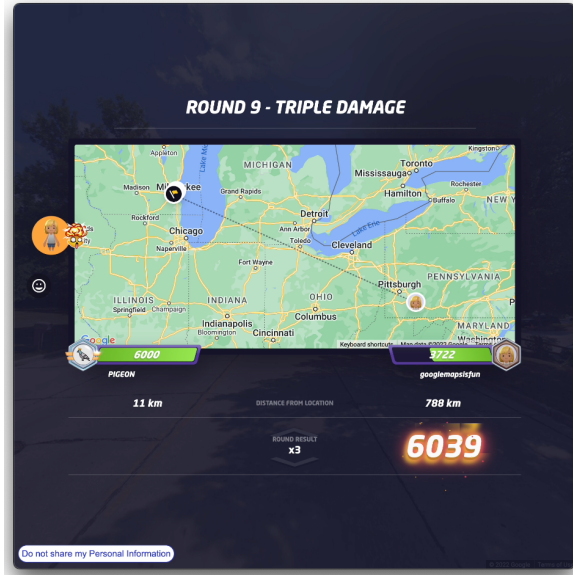
$$\text{score}(x) = 5000 \cdot e^{-\frac{x}{1492.7}}, \quad (3)$$

where x is the prediction error in kilometers.

To get a better sense of the game, we provide some sample screenshots in Figure 22. We took these screenshots while deploying PIGEON in the real GeoGuessr game against real opponents using our self-developed Chrome Extension, which we describe in Section D of this Appendix.



(a) Sample image in a GeoGuessr location.



(b) Sample comparison of guesses between PIGEON and a human player.

Figure 22. Sample screenshots from PIGEON deployed to the GeoGuessr game.

D. Chrome Extension for GeoGuessr

We constructed a Chrome extension that plays GeoGuessr by automating the browser. We did this to achieve two goals: First, having an engaging live demonstration. Second, confirming that our model is robust enough to also perform well on the real-world data from the GeoGuessr game.

D.1. Chrome Extension Behavior

The extension automatically activates itself once it detects that it is in a game and then autonomously places guesses. Moreover, it is able to detect when a game is over and restarts the game automatically if it is configured to do so. At the moment, it supports the following GeoGuessr game modes: Classic, Duel & Team Duel. It is able to play both in the “Play With Friends” and “Competitive” mode. In the latter mode, you are matched online against another player of similar rank, and each game either increases or decreases an Elo-based rank.

The procedure to place a guess works as follows and is repeated for each GeoGeussr round until the game is detected to be over:

1. Resize Chrome window to correct aspect ratio.
2. Wait until Street View scene is fully loaded.
3. Repeat the following for all four directions:
 - (a) Hide all UI elements.
 - (b) Take a screenshot.
 - (c) Unhide all UI elements.
 - (d) Rotate by 90° using simulated clicks.
4. POST request to our backend server endpoint with the four images encoded as Base64 as payload.
5. Receive predicted latitude & longitude from our server.
6. Optional: Random delay to behave more human-like
7. Place guess using reverse-engineered API call from GeoGuessr API.
8. Collect statistics about true location & human performance and submit to the server using an additional POST request.

D.2. Backend

In addition to the Chrome extension, we run a backend server on a machine with a GPU that runs the model inference. We utilize the Python library FastAPI to implement two API endpoints:

1. Inference endpoint: A POST endpoint that receives either one or four images, passes them to a Pytorch pipeline that preprocesses the images, and then runs inference on a GPU. In addition, it saves the images on disk in order to collect an additional dataset. Then, it returns the latitude & longitude of our models to the client.
2. Statistics endpoint: A POST endpoint that receives the statistics about the correct location, the score & distance of our guess, and human performance (i.e., location, score, and distance of our online opponent). This data is saved on disk and then used for our evaluations.

E. Technical Specification

The following is an overview of the technical infrastructure used for this project, an estimation of the time needed to compute our results, and an overview of the most important model parameters.

E.1. Technical Infrastructure

Our geolocalization models were trained on four NVIDIA A100 80GB GPUs with each model training between three hours and two days. The contrastive pretraining of StreetCLIP required a total of eight NVIDIA A100 80 GB GPUs on which we pre-trained our model for two days.

The geocell creation algorithm ran for one day on a local machine on a single CPU.

E.2. Hyperparameter Specification

For all our geolocalization models, we started by freezing all CLIP layers and solely training the prediction heads. To do so, we used a learning rate of $1e^{-4}$ and a batch size (accumulated across GPUs and gradient updates) of 256. Once the prediction heads were trained to convergence we unfroze the last CLIP layer for the respective models and used the same batch size of 256 but lowered the learning rate to $2e^{-5}$.

For the contrastive pretraining of StreetCLIP, we used an batch size of 2048 accumulated across all GPU cores and gradient updates, a learning rate of $1e^{-6}$, linear learning rate warmup with rate 0.2, and a weight decay of 0.001.